2nd CEPHONA Workshop
on Microscopic Characterisation
of Materials and Structures for Photonics

Warsaw, November 22-23, 2004

CROSS-SECTIONAL SCANNING TUNNELING MICROSCOPY OF III-V COMPOUNDS

Bruno GRANDIDIER

Institut d'Electronique, de Microélectronique et de Nanotechnologie, Av. Poincaré BP 69, 59652 Villeneuve d'Ascq cedex, France

ABSTRACT

Lattice imperfections such as doping atoms or intermixing in III-V semiconductor compounds can be studied on an atomic scale with scanning tunnelling microscopy (STM). Due to the ideal properties of the (110) cleaved faces of most of the III-V semiconductor compounds, bulk effects are not screened at the surface and the mechanical distortion of the lattice as well as the electronic structure of the layers can be determined. Here, taking into accounts of the mechanical and electronic contribution in the interpretation of the STM images, acceptor impurities and InAs quantum dots in GaAs are investigated.

INTRODUCTION

Compound semiconductor formed by the group III elements and by the group V elements are among the most outstanding semiconductor materials for optoelectronic applications. As the dimensions of III-V semiconductor devices keep on shrinking, a controlled incorporation of impurities and chemical species during the growth is required to avoid the failure of the devices. Indeed, the required sizes of the active elements in III-V structures are now of the order of 10 nm. Although most of the conventional growth methods, like molecular beam epitaxy, can deposit materials with sub-monolayer precision, it is still challenging to keep free of defects the interfaces between different layers in order to obtain the desired optical or electronic properties. Multilayer and quantum structures are generally grown in the [001] direction and to examine the physical properties of the layers, indirect methods are generally applied. However, when the electronic structure of the layers is deduced by means of optical or electron spectroscopy, the knowledge of the chemical composition or the quality of the interfaces in the layers is missing. Alternatively, electron microscopy allows the observation of their morphology, but does not provide information of the electronic properties of the structures. In contrast to most of these investigation tools, scanning tunnelling microscopy has emerged as a powerful technique to characterize III-V semiconductor structures. Precise characterization of these materials is made possible by the fact that zinc-blende III-V crystals readily cleave along the {110} faces, producing atomically flat surfaces, that present a cross-sectional view of the structures grown on (001) substrates, as shown in the schematic diagram of Fig. 1.

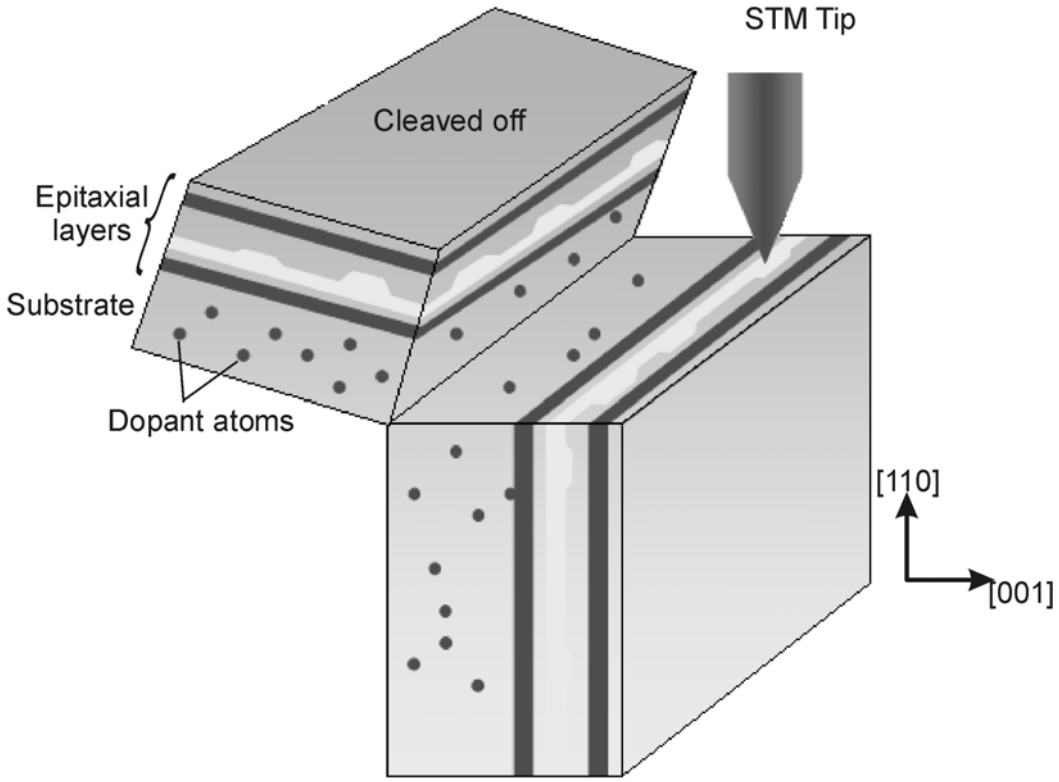

Fig. 1. Principle of cross-sectional scanning tunnelling microscopy (XSTM)

In contrast to transmission electron microscopy (TEM) which yields a cross-section view averaged through many lattice planes, cross-sectional scanning tunnelling microscopy (XSTM) shows a single plane of atoms. Furthermore, the (110) surfaces prepared by cleavage in ultra high vacuum (UHV), are not reconstructed and the contrast obtained in the STM images allow the investigation of surface and bulk properties. However, the interpretation of XSTM images is generally not straightforward. Indeed, as shown in Fig. 2, the contrast of the images is related to both electronic effects through the spatial variation of local density of states in the samples as well as topographic effects measured through the spatial variation of the probability transmission. As III-V semiconductors layers may have different chemical compositions, strain or electronic structures, all these properties must be considered to explain the contrast variation of the images [1]. This short report illustrates these electronic and mechanical contributions to the STM contrast of impurities and quantum dots (QDs) in III-V semiconductor compounds.

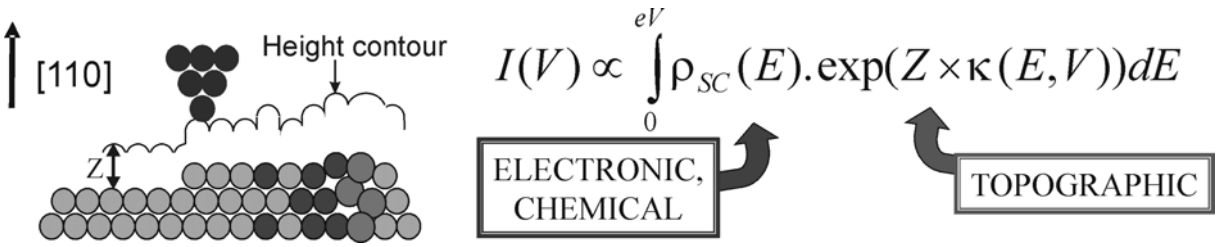

Fig. 2. Topographical and electronic/chemical effects on the Z height contour followed by the tip scanning above the surface. The topographical change are induced by atomic step or strain, whereas the electronic effect are caused by different chemical species or layers with different electronic structures. In the simplified expression of the tunnelling current, $\rho_{sc}(E)$ corresponds to the density of state of the sample; the density of states of the tip is taken as constant. κ is the inverse decay length of the electron in the tunnelling barrier.

1. ATOMIC STRUCTURE OF DEFECT FREE (110) CLEAVED III-V SURFACES

Cubic zincblende structures of III-V semiconductors cleave along their nonpolar (110) planes and these planes exhibit a 1x1 reconstruction, with an equal number of anions and cations on the surface. The cleavage results in two broken bonds in each surface unit cell. To lower its energy, the structure relaxes by a pure bond rotation relaxation, the anion being displaced outward. This buckling effect causes a charge transfer between the surface cations and anions, leaving the III dangling bonds empty and the V dangling bonds filled. Therefore the cations and anions surface states become resonant with the conduction band states and the valence band states respectively, leaving the band gap region free of surface states. Since the semiconductor Fermi level lies generally in the band gap region and only the states lying between the Fermi levels of the semiconductor and the tip contribute to the tunneling process, the III dangling bonds are seen at positive sample bias (empty state image), whereas the V dangling bonds are visible in the negative sample bias (filled state image). Such a result is illustrated in Fig. 3 for the case of a GaAs (110) surface, where the Ga and As atomic lattices are resolved for opposite sample voltages in the STM images. To obtain the true atomic structure of the surface, the voltage dependent images must be thus superimposed.

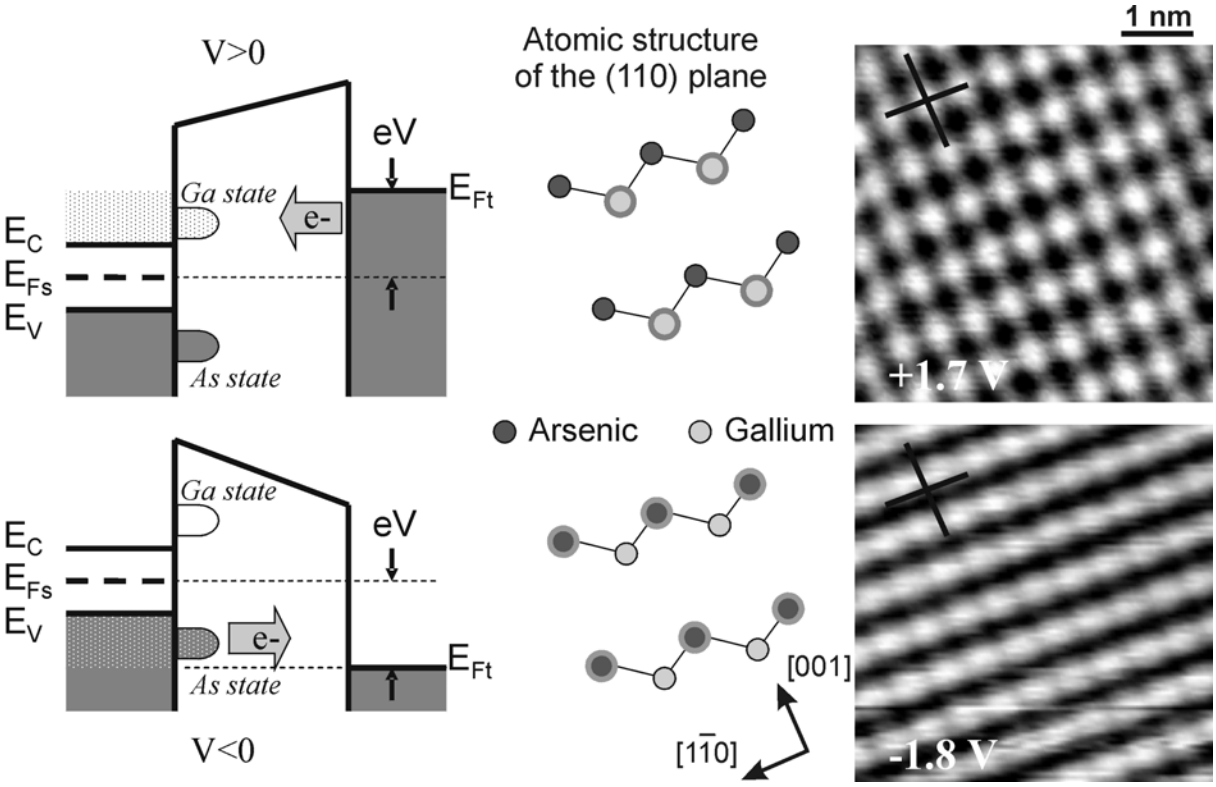

Fig. 3. Voltage dependent STM images of a cleaved GaAs (110) surface. The image obtained at +1.7 V shows the empty Ga surface states, whereas the image obtained at -1.8 V corresponds to the filled As surface states. The tunnelling current is 100 pA for both images. The contribution of the respective states as a function of the voltage applied to the GaAs sample is highlighted by the energy diagram and the thick grey contour surrounding the Ga or As atoms of the (110) surface.

2. ACCEPTOR IMPURITIES OBSERVED BY XSTM

Since defect-free (110) surfaces exhibit the absence of surface states in the band gap and since the cleavage of the crystal takes place in UHV, what preserves the cleanliness of the surface, the identification of dopants can be achieved. Figure 4a shows a typical XSTM image obtained from the cleavage of p-type GaAs single crystals, with a nominal Zn concentration of $2x10^{19}$ $Zn.cm^{-3}$. The image was acquired at a positive sample bias, so that the sample empty states contribute to the

tunnelling current. The Ga background atomic corrugation is clearly seen and numerous elevations, consisting of a triangular shape, are superimposed to the atomic lattice. Their observation reveals several apparent heights and symmetries, suggesting that these elevations correspond to dopant atoms positioned at different depths below the surface [2], as indicated in Fig. 4. Their count gives a dopant concentration of $(1.8 \pm 0.3) \times 10^{19}$ cm^{-3} in good agreement with the expected concentration.

As the contrast variation may be due to a mechanical distortion of the lattice, caused by the difference of atomic radii between Zn (0.83 Å) and Ga (0.62 Å) atoms, cross-sections of GaAs crystal doped with smaller radius impurities have been investigated. As shown in Fig. 4b, Be impurities give rise to triangular protusions instead of depressions. As a result, the contrast observed in the STM images of acceptor impurities must be electronic, because strain would yield significant differences between Be and Zn in contrast to the observations.

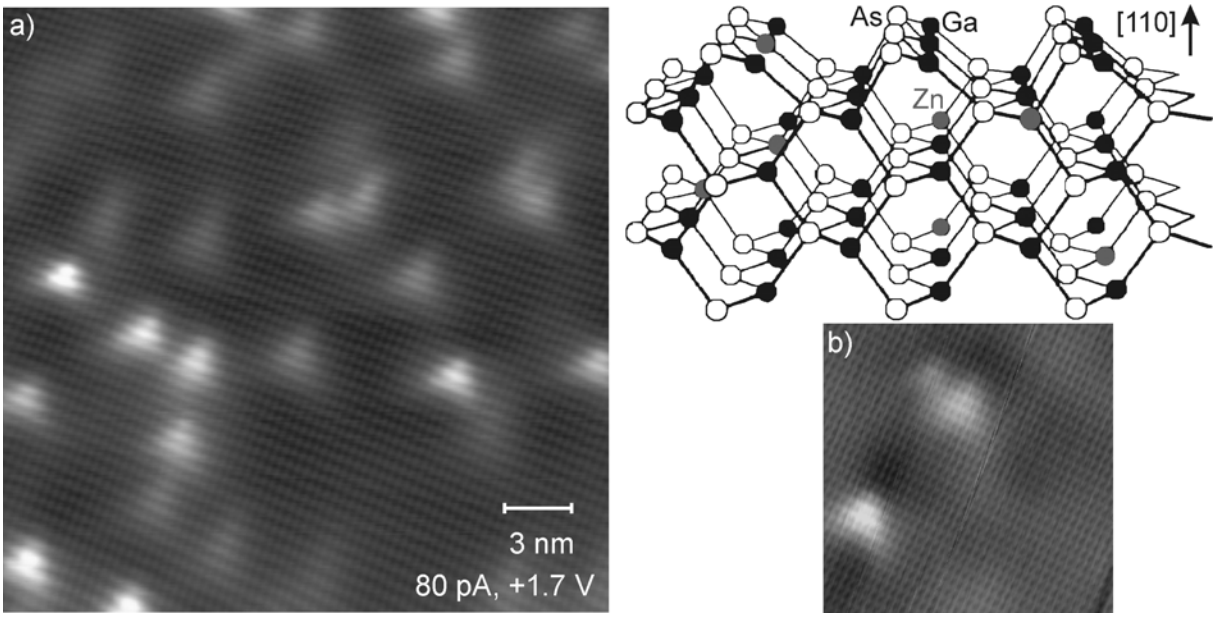

Fig. 4. a) STM image of a Zn-doped GaAs(110) surface, acquired at a temperature of 4.8 K. The triangular shapes superimposed to the atomic lattice show different types of intensity and symmetry. They reflect the presence of acceptor dopants incorporated in different planes as illustrated by the Zn dopants in the crystals drawn at the right of the image. b) STM image of a Be-doped GaAs(110) surface, acquired with the same conditions as in a).

3. InAs QUANTUM DOTS IN GaAs

Spontaneous emission control using solid-state microcavities has been the object of intense research activity. While the available emitters made up of quantum wells are much broader spectrally than the resonant modes of these cavities, the quantum dots can exploit the full potential of high Q cavities for spontaneous emission control due to their small spectral widths. InAs QDs were inserted in the central part of GaAs/AlAs micropillar, as shown in Fig. 5. The QDs were grown by molecular beam epitaxy on a (001) oriented GaAs substrate. In order to build each dot array, 2.3 monolayers of InAs were deposited on the GaAs layer within 20 s at a temperature of 520 °C. They were immediately buried with GaAs. With these growth conditions, the density of dots is as high as 10^{10}cm^{-2} in the (001) plane and a large number of InAs QDs cross-sections can be observed. In the STM image of Fig. 5, the QDs appear bright and the GaAs layers dark.

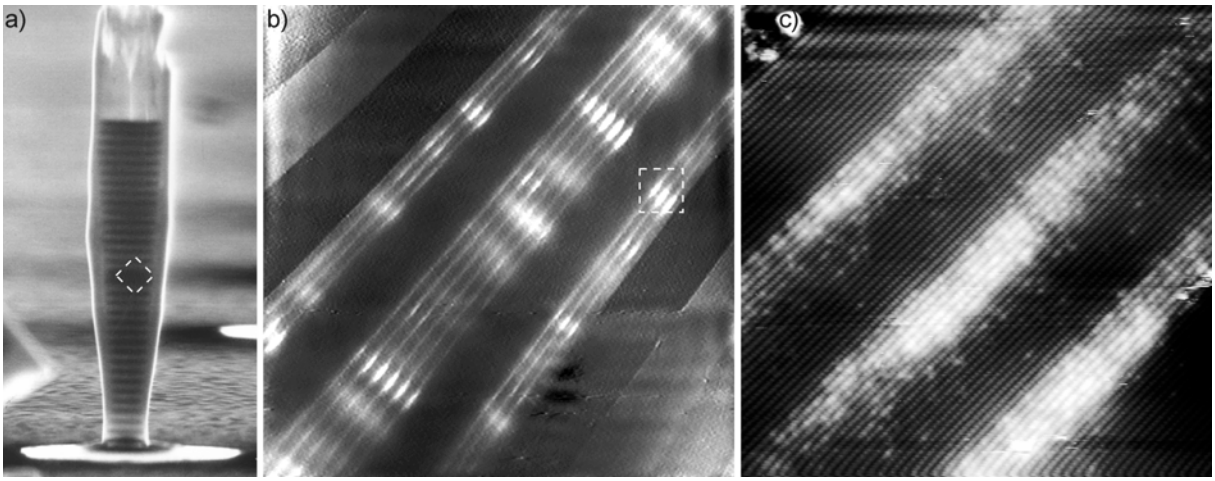

Fig. 5. Sequence of zooms into the active element of a solid state emitter. The zoomed areas are outlined by a dashed square. a) Scanning micrograph obtained for a 1 μm diameter micropillar containing InAs QDs. The top and bottom distributed Bragg reflectors are clearly visible; the array QDs has been inserted in the middle of the central cavity. b) STM image of the cleaved central cavity showing AlAs/GaAs layers surrounding the 12 (3,6,3) QD arrays. The QDs are self-aligned inside each group of QD arrays. Image size: 500 x 500 nm^2 c) STM image of three QDs at the atomic resolution. Bright atoms can be seen in the GaAs layers between the QD arrays, indicating In segregation. Sample voltage: +2.3V, tunnelling current : 100 pA.

The contrast of the STM images depends on both the topographic variations of the surface and the electronic structure of the underlying layer. As the InAs QDs are compressively strained in GaAs, the (110) cross section of a QD is likely to be displaced outward due to the relaxation of the materials after the cleavage [3]. Such displacement causes a bright contrast in the STM images in agreement with the observed contrast in Fig. 5. However, the density of states in the QDs is higher than the one in the GaAs layer when energies below or at the bottom of the GaAs conduction band edge are probed. At low sample voltages, their contribution is thus significant in the tunneling current and to keep the tunneling current constant, the tip is retracted when it scans a QD, what induces also a bright contrast in the STM image. To estimate the relative contributions of both effects, the mechanical effect can first be determined by calculating the strain relaxation in cleaved InAs dots embedded in GaAs [4]. Such a calculation considers a truncated pyramid like InAs dot, with a 20 nm [100]x[010] square base and {110} faces, lying on a 0.4 nm thick wetting layer as seen in Fig. 5. The cleavage surface splits the dot along the main diagonal of the square base. The strain relaxation at the cleaved edge is calculated with a finite difference method within the continuum elasticity theory and is shown in Fig. 6a. When the calculated structural height variation at the cleavage surface due to the strain relaxation is compared with the contour line plot obtained from dots on the STM image (Fig. 6b), a height variation of 4 Å is found for voltages higher than +1.86 volt. Therefore, in contrast with the acceptor impurities in GaAs, the strain relaxation is the major source of contrast between the dot and the surrounding layer for such a voltage range.

Due to their reduced sizes, the dots exhibit a three dimensional confinement with a δ-function-like electronic density of states. As the electron ground and first excited states in these dots are generally separated by a few tens of meV, the energy of both states can be resolved by tunneling spectroscopic techniques at room temperature. Since the (110) surfaces are electronically unpinned, tunneling spectroscopy allows the determination of the bulk electronic properties, such as the band gap or the electron subbands of quantum wells [5]. Furthermore, in the case of the QDs, at positive samples higher than +1.8 V, the tip to sample distance can be considered as being the same when the tip is located either above a dot, the wetting layer or the GaAs spacers. Thus, the sensitivity of the spectroscopic measurements does not depend strongly on the tip-sample separation, but rather on the spatial variation of the sample density of states.

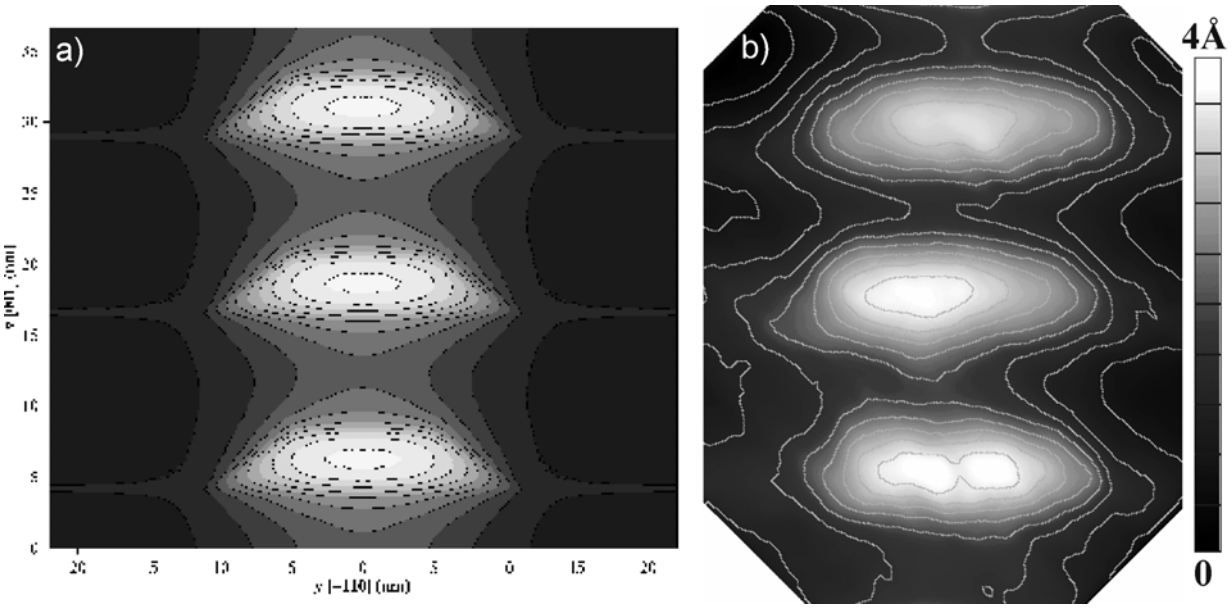

Fig. 6. Comparison of the height variation between a) a simulated topographical image and b) a STM image of cleaved InAs dots acquired with a sample voltage of +2.1V. The grey scale is displayed in the vertical bar. A low pass filter was used to remove the atomic corrugation from b). For clarity a contour line is displayed in the images.

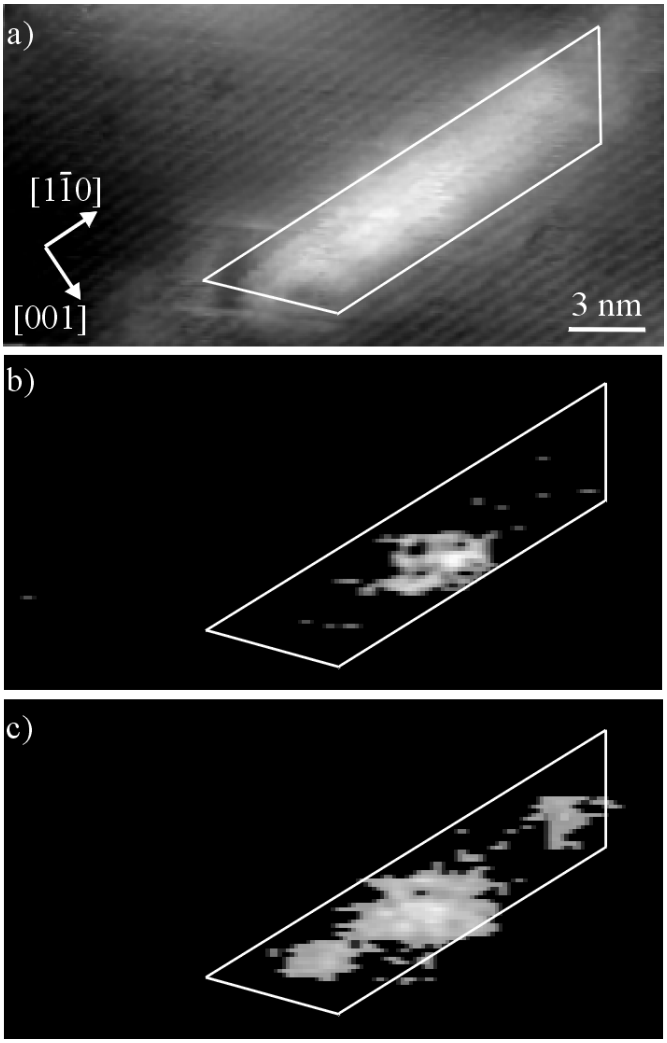

Fig. 7. Simultaneously acquired topographic and current images of an InAs Qs: (a) STM topograph acquired with a sample voltage of +2.15 V, current images at a sample bias of (b) +0.69 V and (c) +0.82 V. The boundaries of the box, determined from figure (a), are outlined in each image. The grey scale ranges from 0.01 pA to 0.8 pA and 1.5 pA for figures (b) and (c) respectively.

To investigate the electronic structure of a dot, tunneling current voltage curves were acquired simultaneously with the topographic image above individual quantum dots. At every points of the image, obtained with a sample voltage of +2.15 volts, the feedback loop was switched off to measure I-V curves. During an I(V) measurement, the vertical position of the tip is held stationary. A current image at a given voltage is then drawn by plotting in each point of the image the value of the current obtained at this point during the I-V measurement. The results are displayed in Fig. 7. Figure 7(a) is the topographic image of a QD. This particular dot has a base length of 20 nm and a height of 4 nm. The current images are displayed in Fig. 7(b) and 7(c). They were obtained for an applied voltage of +0.69 V and +0.82 V respectively. In these images, regions of high current are bright and regions of low current are dark. While Fig. 7(a) outlines the dot contour, the current image in Fig. 7(b) shows a standing wave pattern in the center of the dot. The intensity of this feature varies with voltage: it becomes clearly visible at a voltage of +0.63 V and its intensity increases up to +0.74 V. At a voltage of +0.74 V, the standing wave pattern suddenly changes. Two new features are now apparent surrounding the central feature in the $[1\bar{1}0]$ direction, as shown in Fig. 7(c). Their intensity increases with voltage up to +0.9 V. For sample voltages larger than +0.9 V, the dot becomes brighter and brighter with no other distinct feature visible in the dot. For such large voltages, we may expect to tunnel into the empty states of the wetting layer and the GaAs conduction band [6].

As it was previously shown that the tip-sample separation is insensitive to the electronic effects for a voltage of +2.15 volts, the wave patterns in Fig. 7(b) and (c) are obtained without the interference of mechanical contributions and so reflect the spatial distribution of the lowest electron states confined in the dot. As only the states lying between the Fermi levels of the sample and of the tip contribute to the tunneling process, the standing wave pattern at a voltage of +0.69 V corresponds therefore to the probability density of the electron ground state in the dot, whereas at a voltage of +0.82 V, the standing wave pattern can be regarded as a combination of the probability densities of the electron ground and first excited states, where the ground state exhibits the s-like symmetry and the first excited state the p-like symmetry with one nodal plane.

Acknowledgment

The author is grateful to G. Allan, C. Delerue, D. Deresmes, J.M. Gérard, B. Legrand, Y.M. Niquet, G. Mahieu, J.P. Nys, C. Priester, D. Stiévenard, V. Thierry-Mieg, who contributed in various ways to this work.

Email address: grandidier@isen.iemn.univ-lille1.fr

[1] B. Grandidier, R.M. Feenstra, C. Silfvenius, G. Landgren, J. Vac. Sci. Technol. A17, 2251 (1999).
[2] Ph. Ebert, Surf. Sci. Rep. 33, 121 (1999).
[3] B. Legrand, B. Grandidier, J.P. Nys, D. Stiévenard, J.M. Gérard, V. Thierry-Mieg, Appl. Phys. Lett. 73, 96 (1998).
[4] M. Grundmann, O. Stier, D. Bimberg, Phys. Rev. B 52, 11969 (1995).
[5] R.M. Feenstra, D.A. Collins, D.Z.Y. Ting, M.W. Wang, T.C. McGill, Phys. Rev. Lett. 72, 2749 (1994).
[6] B. Grandidier, Y.M. Niquet, B. Legrand, J.P. Nys, C. Priester, D. Stiévenard, J.M. Gérard, V. Thierry-Mieg, Phys. Rev. Lett. 85, 1068 (2000).